The Journal of Supercritical Fluids 237 (2026) 107055

Contents lists available at ScienceDirect

The Journal of Supercritical Fluids

journal homepage: www.elsevier.com/locate/supflu

Quantitative measurement of pseudo-vapor-layer thickness and its contribution on supercritical heat transfer

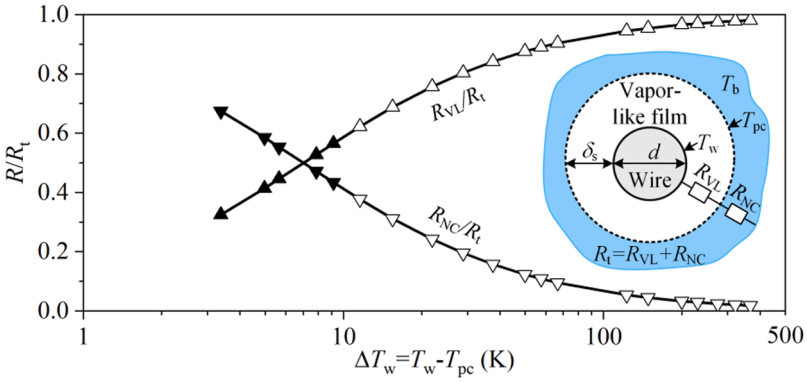
Bo Zhang [a], Jinliang Xu [a,*], Xiongjiang Yu [b], Jian Xie [b], Guanglin Liu [a]

[a] Beijing Key Laboratory of Multiphase Flow and Heat Transfer for Low Grade Energy Utilization, North China Electric Power University, Beijing 102206, China
[b] Key Laboratory of Power Station Energy Transfer Conversion and System of Ministry of Education, North China Electric Power University, Beijing 102206, China

HIGHLIGHTS

- Immersion heat transfer of supercritical carbon dioxide was investigated.
- Pseudo-vapor-layer thickness was measured using the grey extraction method.
- Natural convection dominates heat transfer at very small wall superheating.
- Pseudo-vapor-layer dominates heat transfer at ultra-high wall superheating.
- Mixed mechanism of natural convection and pseudo-vapor-layer heat transfer at moderate wall superheating.

GRAPHICAL ABSTRACT



ARTICLE INFO

Keywords:
Pseudo-boiling
Natural convection heat transfer
Evaporation-like heat transfer
Pseudo-vapor-layer thicknesses

ABSTRACT

Here, we measure the pseudo-vapor-layer thickness of supercritical heat transfer. Experiments were carried out by heating a horizontally positioned 70 μm diameter and ~28 mm length platinum wire immersed in a carbon dioxide pool having three pressures of 7.6 MPa, 9.0 MPa and 11.0 MPa, respectively. The direct photographic technique ensures capture of the vapor-liquid interface by the grey extraction method. The pseudo-vapor-layer thicknesses are shown to decrease with increase of irradiance intensities of the LED light but a saturation value can be reached. Covering a wide heat flux range of (1−800) kW/m^2, the "boiling" curve includes a natural convection region at small wall superheating of $\Delta T_w < 10$ K, and an evaporation-like region with ΔT_w in a range of (10−420) K. In the natural convection region, both heat transfer coefficients and pseudo-vapor-layer thicknesses increase with increases of wall superheating. In the evaporation-like region, heat transfer coefficients decrease to be constant but pseudo-vapor-layer thicknesses continuously increase. Under the extreme conditions of small and ultra-high wall superheating, natural convection and pseudo-vapor-layer dominate the heat transfer, respectively. In the moderate wall superheating, the heat transfer behaves as the mixed mechanism of natural convection and pseudo-vapor-layer heat transfer. A non-dimensional parameter is proposed to characterize the pseudo-vapor-layer heat transfer effect. The pseudo-vapor-layer conduction assumption overestimates the pseudo-vapor-layer resistance. Our work presents the quantitative measurement of the pseudo-vapor-layer, highlighting the significance of the pseudo-vapor-layer on heat transfer in supercritical pressures.

* Corresponding author.
E-mail address: xjl@ncepu.edu.cn (J. Xu).

https://doi.org/10.1016/j.supflu.2026.107055
Received 22 January 2026; Received in revised form 4 April 2026; Accepted 31 May 2026
Available online 1 June 2026
0896-8446/© 2026 Elsevier B.V. All rights are reserved, including those for text and data mining, AI training, and similar technologies.

Nomenclature

Symbols

A	coefficient related to polarizabilities (m3/kg)
C	grey level
$\widehat{C}$	non-dimensional grey level
d	diameter of wire (μm)
D	diameter of shadow area (μm)
G	mass flux (kg/s)
h	heat transfer coefficient (kW/(m2·K))
i	enthalpy (J/kg)
I_c	radiation fluxes (kW/m2)
K	non-dimensional parameter
L	length of wire (mm)
LP	light power (W)
n	refractive index
Nu	Nusselt number
P	pressure (MPa)
q	heat flux (kW/m2)
Q	heating power (W)
R	electrical resistance (Ω)
Ra	Rayleigh number
SBO	supercritical-boiling-number
T	temperature (K)
V	voltage (V)

Greek symbols

β	pseudo-vapor-layer contribution ratio
δ	thickness (μm)
δ_s	steady-state thickness (μm)
λ	thermal conductivity (W/(m·K))
ρ	density (kg/m^3)
$\overline{\rho}$	electrical resistivity (Ω ·m)

Subscripts

ave	average
b	bulk
c	critical
max/min	maximum/minimum
NC	natural convection
pc	pseudo-critical
s	standard resistance
sat	saturation temperature
t	total
VL	pseudo-vapor-layer
VL,con	the conduction of pseudo-vapor-layer
w	wall

Abbreviations

DC	direct-current
HTD	heat transfer deterioration
NHT	normal heat transfer
sCO_2	supercritical carbon dioxide
SHT	supercritical heat transfer
TPL	two-phase-like

1. Introduction

For a long history, supercritical fluid is treated as a single-phase fluid without bubbles, droplets and interfacial phenomenon [1]. Supercritical heat transfer (SHT) is correlated considering the buoyancy effect and acceleration effect [2,3]. Now, it is known that although great effort has been taken by introducing modification parameters to improve the prediction accuracies, large deviation exists between predicted heat transfer and measured values, based on the single-phase fluid framework [4,5]. It is noted that none of available heat transfer correlations match experimental data well [6], and heat transfer deterioration (HTD) is difficult to be explained and correlated in a classical way [7].

In the 1950s, convective heat transfer was conducted in supercritical domain with water as the working fluid, which was initiated to develop high efficiency nuclear and coal-fired power plants [8]. Wall temperatures were measured under a constant heat flux boundary condition. The HTD leads to a sharp peak in wall temperatures before the fluid reaches the pseudo-critical temperature [4]. Because HTD is strongly related to the facility safety, it is important for practical applications. Now that HTD cannot be explained by the single-phase fluid theory, the *pseudo-boiling* term was introduced by linking the similar phenomenon in supercritical pressure and subcritical pressure [9,10].

Since the proposal of the term, pseudo-boiling has not been paid great attention, but progress has been achieved in recent years. Gallo et al. [11] studied thermodynamic properties of supercritical water by analysing available experimental data and computer simulation results, indicating that the Widom line coincides with a crossover from a liquid-like to a gas-like behavior in transport properties. With neutron imaging techniques, density fluctuations of supercritical water are monitored while the system evolves rapidly from liquid-like to gas-like during isobaric heating, showing different responses in the two separated regions when crossing the Widom line [12]. Banuti [13] developed the phase transition temperatures when crossing the Widom line from liquid-like to gas-like fluid states. The connection between thermodynamic conditions and microstructural behavior was studied by utilizing a first-principles-based criterion and self-similarity analysis [14]. Energetically localized molecular clusters whose size distribution and self-similarity are identified in supercritical phase space, showing the structural response of these clusters following a complex network behavior whose dynamics arises from the energetics of isotropic molecular interactions [14].

In contrast to sharp transition from liquid-like region to gas-like region interfaced at the Widom line, the supercritical domain is decoupled into three regimes by adding a two-phase-like (TPL) region, which is identified by molecular dynamics simulations [15]. The observed nanovoids are very similar to bubbles in subcritical pressure, thus they are called *bubble-like*. Nonlinear dynamics demonstrates chaotic behavior in the TPL regime, highlighting the multiphase feature of supercritical fluid [15]. Direct classification of liquid-like and gas-like molecules coexisting in the supercritical fluid is identified by machine learning analysis [16]. The deltoid coexistence region encloses the Widom line and may therefore be termed the Widom delta [16]. Wang et al. [17] developed a three-regime model. Considering convective heat transfer in tubes, the three regimes of liquid-like, two-phase-like and gas-like are plotted along flow direction. Attention was paid on the determination of physical properties in the TPL regime. The vapor mass quality x is defined to represent the mass fraction of the vapor-like fluid with respect to the total mixture mass. They found that SHT deviates from single-phase convection heat transfer significantly within $0 < x < 1$ [17].

To develop high performance supercritical carbon dioxide (sCO_2) power cycles, investigations have been performed using CO_2 recently. Under heating condition, supercritical fluid is assumed to have a pseudo-

vapor-layer near the wall and a liquid-like fluid in the tube core [18–20]. Similarity analysis between subcritical boiling and SHT creates a new dimensionless parameter, the *K* number, representing the evaporation induced momentum force relative to the inertia force to govern the growth of pseudo-vapor-layer thicknesses, revealing sudden changes from normal heat transfer (NHT) to HTD with obvious temperature peak when crossing a critical supercritical boiling number *(SBO)*, which is 5.126×10^{-4}, 2.018×10^{-4}, 1.653×10^{-4} and 1.358×10^{-4} for CO_2, H_2O, R134a and R22, determined by a large quantity of experiment database [19]. The *K* number is further used to develop a general heat transfer correlation in a very simple form, demonstrating better accuracies by comparing with other correlations reported in the literature [20]. Nieuwenhuyse et al. [21] demonstrated that the heat transfer prediction accuracies are improved by adding the *SBO* term when dealing with supercritical heat transfer in horizontal tubes. Pu et al. [22] developed a new correlation by including a term characterizing the pseudo-boiling effect, the *K* number. Promising findings on understanding the complicated heat transfer behaviors and improvement of the heat transfer predictions have been achieved [22].

It is known that there are two modes of evaporation and boiling in subcritical pressures. The former takes place at available vapor-liquid interface but the latter creates new interface [23]. He et al. [24] studied the two modes of heat transfer in supercritical pressures. They found the evaporation-like heat transfer beyond the natural convection limit when using a platinum wire as the heater and temperature sensor. However, both the evaporation-like and boiling-like modes take place covering wide range of heat fluxes when using a thin NiCr wire. The generation of pseudo-bubbles in the boiling-like region is either caused by the piston motion of the heater wire, or caused by the spatial-temporal temperature variations of the heater wire. The piston motion refers to the periodic movement of the heating wire in the vertical direction [24]. By processing image files, pseudo-boiling contributes 19%−65% to the total heat transfer, indicating the significance of the pseudo-boiling effect [25].

Now that available studies show the importance of pseudo-boiling, an important question is asked that where is the vapor-liquid interface during heating of a supercritical fluid? Once the interface is known, pseudo-vapor-layer thicknesses for the evaporation-like heat transfer, or pseudo-bubble for the boiling-like heat transfer, can be determined. Previous studies used the schlieren or shadowgraph approach to capture images, which highlights the fluid density gradients instead of the interfacial measurement [26,27]. The captured images are blurry after passing through a set of lens, thus they are only used for qualitative analysis.

Here, we measure the pseudo-vapor-layer thicknesses by applying the direct photograph technique incorporating the grey extraction approach. The vessel chamber had three pressures of 7.6 MPa, 9.0 MPa and 11.0 MPa, which are significantly larger than the critical value of 7.377 MPa for CO_2. Covering a wide range of wall superheating from negative to 420 K, two regions of natural convection and evaporation-like region appear, with the former referring to very small wall superheating, but the latter involving a wide range of (10−420) K. The connection between the measured pseudo-vapor-layer thicknesses and heat transfer are established, concluding important contribution of the pseudo-vapor-layer on the heat transfer.

Even though many studies are available on natural convection heat transfer [28,29], the phenomena are not well understood in supercritical pressures. Classically, supercritical fluid is treated as a single-phase fluid [1]. In this paper, the measurement of pseudo-vapor-layer thickness is helpful in developing a new measurement technique within a multiphase fluid framework, highlighting interfacial effects in supercritical pressures. Due to the wide applications of supercritical fluids in the fields of thermal-power conversion [30], electronic cooling [31], nanomaterial synthesis [32], and waste water treatment [33], the experimental results of this paper can be compared with future numerical simulations using an interface tracking method such as volume-of-fluid (VOF) in supercritical pressures. Inspired by the findings of this paper, new heat transfer correlation will be developed emphasizing the pseudo-vapor-layer effect.

2. Experimental system and method

2.1. Experimental system

Fig. 1a shows the experimental setup, consisting of a pressure stabilizer system (1−4), a temperature stabilizer system (10, 11), a high-pressure vessel (12), a heater wire test Section (5, 8, 13), a high-speed camera system (9, 14, 15), and a data acquisition system (6, 7). Before charging CO_2 fluid in the pressure vessel, non-condensable gas was removed out of the vessel by continuously flushing CO_2 gas through the vessel. The vessel is connected with a CO_2 gas bottle. Via regulating a precise pressure control valve, the pressure in the vessel is stabilized to a specific value, which is higher than the critical pressure of 7.377 MPa for CO_2. A helical coiled tube with cold water flowing inside was immersed in the CO_2 fluid, cooling the CO_2 fluid to reach the temperature below the pseudo-critical temperature. Two sapphire glass windows arranged on the left side and right side of the pressure vessel ensures light passing through the CO_2 fluid for flow visualization. A jacket thermocouple penetrates the pressure vessel to measure the bulk temperature of CO_2. A platinum wire was horizontally positioned and perpendicular to the axial direction of the pressure vessel (see Fig. 1b-c). The wire was connected to an external electric circuit to act as a heat source and temperature sensor. The wire was tightly fixed by the two electrodes via a DC (direct-current) voltage was applied, hence the wire was straight without bending at room temperature. The wire had a diameter of 70 μm and a length of 27.7 mm.

In this work, the CO_2 fluid with a purity of 99.999% was used. The experimental setup ensures precise control of pressure and bulk fluid temperature of the pressure vessel. For example, for an expected pressure of 8 MPa and a bulk fluid temperature of 288.2 K, the real values are controlled to be within the ranges of (7.962–8.025) MPa for pressure and (288.1–288.3) K for temperature, respectively. Our experiments involve three pressures of 7.6 MPa, 9.0 MPa and 11.0 MPa, and two bulk fluid temperatures of 288.2 K and 306.2 K, respectively. Before formal experiment, a careful calibration yields the relationship between the resistivity ($\overline{\rho}_{pt}$) and wall temperature (T_w) of the heater wire as

$$\overline{\rho}_{pt} = \rho_0(1 + a_0 T_w) = 2.227 \times 10^{-8} \times (1 + 0.016 T_w) \quad (1)$$

Note that the unit of T_w is K.

Fig. 2 shows the connection logic of various loops for experiment. A DC power generator supplies a DC voltage on the heater wire, noting that a reference resistance 2 was serially connected in the loop. The cooling water is circulated by a circulation pump, then flows through a temperature control unit via which the outlet temperature of the cooling water keeps constant, and enters the helical coiled tube. Hence, the bulk fluid temperature can be stabilized in the pressure vessel. During experiment, a LED light source iridates the CO_2 fluid via two glass windows. The images are captured by a high-speed camera (Keyence VW−9000, Japan), having a recording rate of 4000 frames per second. The pressure and temperature transducers output voltage signals. All the voltage signals including the voltage applied on the resistance were collected by a high-speed data acquisition system (Yokogawa DL750, Japan) with a sampling rate of 4000 Hz. A synchronizer (MotionPro Timing Hub, IDT, USA) coordinates the data acquisition system and the high-speed camera simultaneously.

2.2. Heat transfer data reduction

For each case, the total voltage and the voltage across the resistance 2 are measured and recorded as V_t and V_s, respectively. The resistance 2 is a standard resistance to have a known value of R_s. Hence, the heater

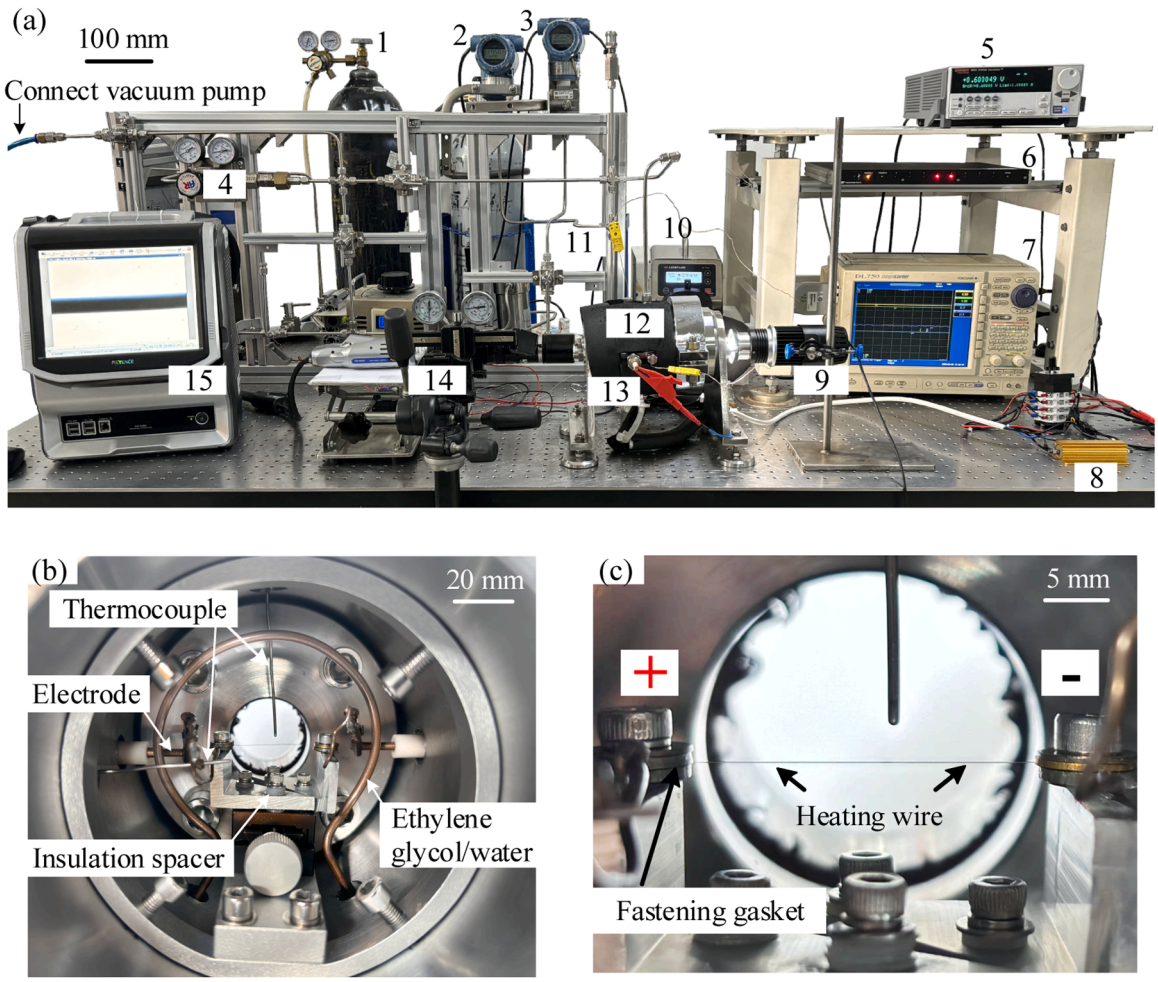


Fig. 1. Experimental setup. (a) Photo of the experimental setup (1. high purity carbon dioxide bottle, 2. pressure transmitter, 3. vacuum transmitter, 4. vent valve, 5. DC power supply, 6. synchronizer, 7. high speed data acquisition system, 8. reference resistance, 9. LED light source, 10. circulating pump, 11. thermocouple, 12. high pressure vessel, 13. electrode, 14. high speed camera, 15. display of high-speed camera); (b) Image focusing on internal structure of the high-pressure vessel; (c) Fixing details of platinum wire.

resistance R and the heating power Q are

$$R = \frac{V_t - V_s}{V_s} R_s \tag{2}$$

$$Q = \frac{V_t - V_s}{R_s} V_s \tag{3}$$

The heat flux based on the outer heater surface area is

$$q = \frac{V_t - V_s}{\pi d L R_s} V_s \tag{4}$$

and the specific resistance of the heater wire is

$$\overline{\rho}_{pt} = \frac{\pi d^2}{4L} \frac{V_t - V_s}{V_s} R_s \tag{5}$$

Where L and d are the heater length and diameter, respectively. Substituting Eq. (5) into Eq. (1) yields the heater temperature of T_w. The heat transfer coefficient h is determined as

$$h = \frac{q}{T_w - T_b} \tag{6}$$

Where T_b is the bulk fluid temperature.

2.3. Measurement of pseudo-vapor-layer thicknesses

In subcritical pressures, it is easy to capture vapor-liquid interface due to sharp transition from liquid to vapor [34]. In supercritical pressure, the measurement of pseudo-interface is seldomly reported. Previously, the schlieren photography and shadowgraph methods were used to capture flow field, challenging on the quantitative identification of the vapor-liquid interface [24]. This is because when light passes through a series of lenses and mirrors, light intensity becomes weakened.

Here, a direct photography method defines the vapor-liquid interface to determine the pseudo-vapor-layer thickness. A LED light source irradiates the supercritical fluid via two glass windows of the pressure vessel. A high speed camera captures the light information. In the CO_2 fluid with a uniform density field without heating on the heater wire, linear relationship is observed between radiation fluxes I_c and the LED light power LP (see Fig. 3a), where I_c is measured by a high precision radiation flux meter (HP330, Shuangse Yunpu, China). Then, the relationship is obtained between the grey values processed by the image file and the radiation fluxes. The grey values cover a range of 0–255, where 0 and 255 represent pure black and pure white, respectively. They are shown to increase linearly with increase of I_c, but reach a saturation value of 255 beyond a transition point (see Fig. 3b). This saturation phenomenon will be explained later.

Heating the wire generates a varied density field of the fluid. A low-

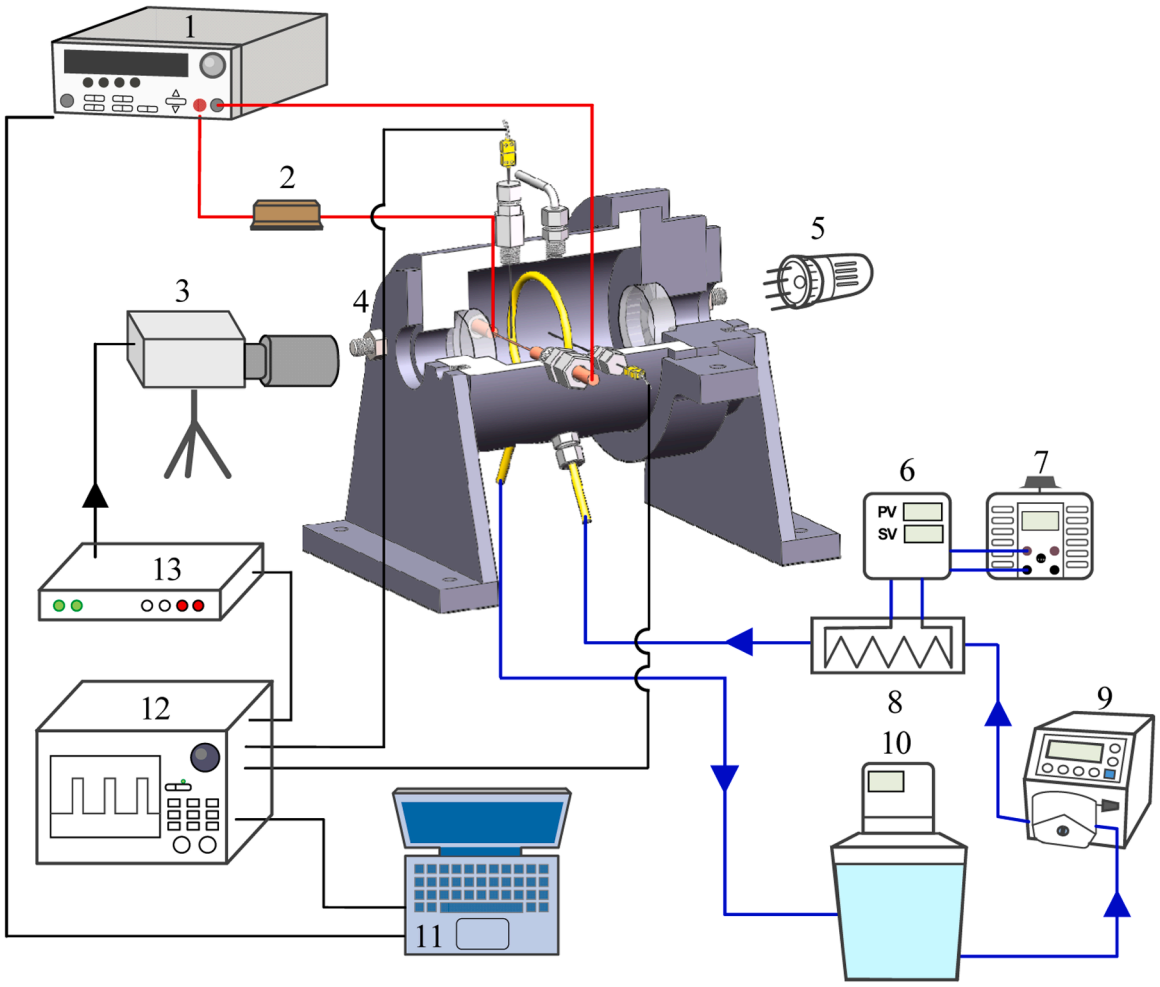


Fig. 2. Signal connection of the sCO_2 heat transfer system. (1. DC power supply, 2. reference resistance, 3. high-speed camera, 4. high pressure vessel, 5. LED light, 6. PID temperature controller, 7. AC power supply, 8. heat exchanger to regulate temperature of the circulating fluid, 9. circulating pump, 10. water tank, 11. laptop, 12. high speed data acquisition system, 13. synchronizer).

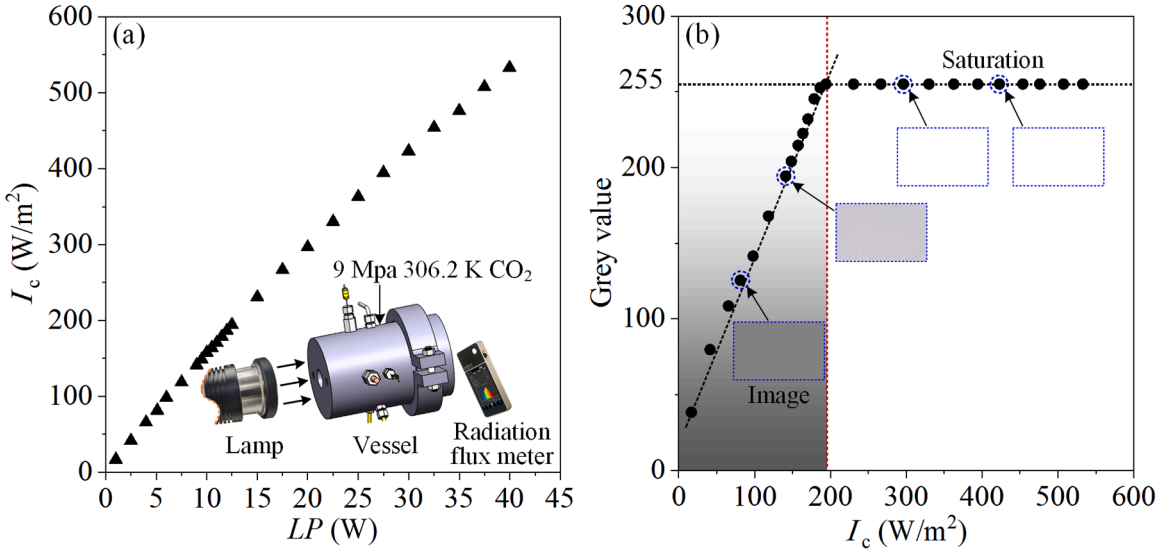


Fig. 3. Effect of light power LP on irradiance density I_c (a) and image grey value (b).

density pseudo-vapor-layer exists near the wire, whereas a high-density fluid exists at a certain distance away from the wire. The refractive index n influences the deflection angle with respect to the horizontal axis. The relationship between n and the fluid density ρ is [35]

$$n = \sqrt{1 + \frac{3A}{\frac{1}{\rho} - A}} \tag{7}$$

For the nonpolar molecule CO_2, the parameter A is a temperature-independent constant with a value of 1.42×10^{-4} m^3/kg [35]. Fig. 4a presents image files for a typical run of $P = 9$ MPa, T_b= 306.2 K, $q = 302.2$ kW/m^2 and T_w= 435.7 K, which are taken using different irradiation fluxes of I_c, or say light power. For each image, the vapor-liquid interface is determined using the grey extraction method. An image file is converted into a 640 × 480 matrix, with each element in the matrix representing a grey value recorded as C, covering a range of (0−255). The non-dimensional grey is defined as [24]

$$\widehat{C} = \frac{C - C_{min}}{C_{max} - C_{min}} \tag{8}$$

where C_{max} and C_{min} are the maximum and minimum grey values for each image, respectively, where $\widehat{C} = 0$ and $\widehat{C} = 1$ represent the light completely shadowed by the wire and the brightest point, respectively. To process image files, a vertical coordinate z is defined to be perpendicular to the wire length direction. Fig. 4b shows the non-dimensional $\widehat{C}$ versus z at different I_c. The location of $\widehat{C} = 1$ defines a black region interface covering a width of D. Hence, the pseudo-vapor-layer thickness is determined as δ= (D-d)/2, where d is the heater wire diameter. Fig. 4c plots the effect of irradiation fluxes I_c on the pseudo-vapor-layer thickness δ and temperature at the vapor-liquid interface T. It is seen that δ decreases from 73.4 μm at I_c= 141.11 W/m^2 to 35.1 μm followed by not variation trend beyond I_c> 300 W/m^2, which is called the saturation pseudo-vapor-layer thickness. The saturation value is used for heat transfer analysis in the latter section.

The saturation phenomenon is related to the optical response of the camera, which is sensitive to the incident light intensity, or say irradiation flux. When I_c is low such as 100 W/m^2 (see Fig. 5a), due to the light path deviation from the horizontal line, the camera cannot receive sufficient light signal within a larger black region, thus a thicker pseudo-vapor-layer is detected. Fig. 5b shows that the black region including the wire and pseudo-vapor-layer is narrowed with increase of I_c, generating a decreased δ⊡ This decrease trend continues until a critical I_c is reached at 300 W/m^2, beyond which the measured δ does not change anymore (see Fig. 5c). Because different camera holds different optical response with respect to incident light power, the saturation characteristic ensures identical saturation value of the pseudo-vapor-layer thickness using different cameras.

2.4. Uncertainties of various parameters

The signals of V_s, V_t and T_b were recorded by a high-speed data acquisition system at a recording rate of 4000 Hz. Here, natural convection heat transfer and evaporation-like heat transfer modes are detected, under which stable heat transfer is achieved. Thus, in fact, the high-speed data acquisition is not necessary. The voltage measurements involved a resolution of 1 mV and a relative error of 0.015%. T_b had an uncertainty of 0.2 K. P was measured using a Rosemount 3051 pressure transducer with a response time shorten than 100 ms and an uncertainty

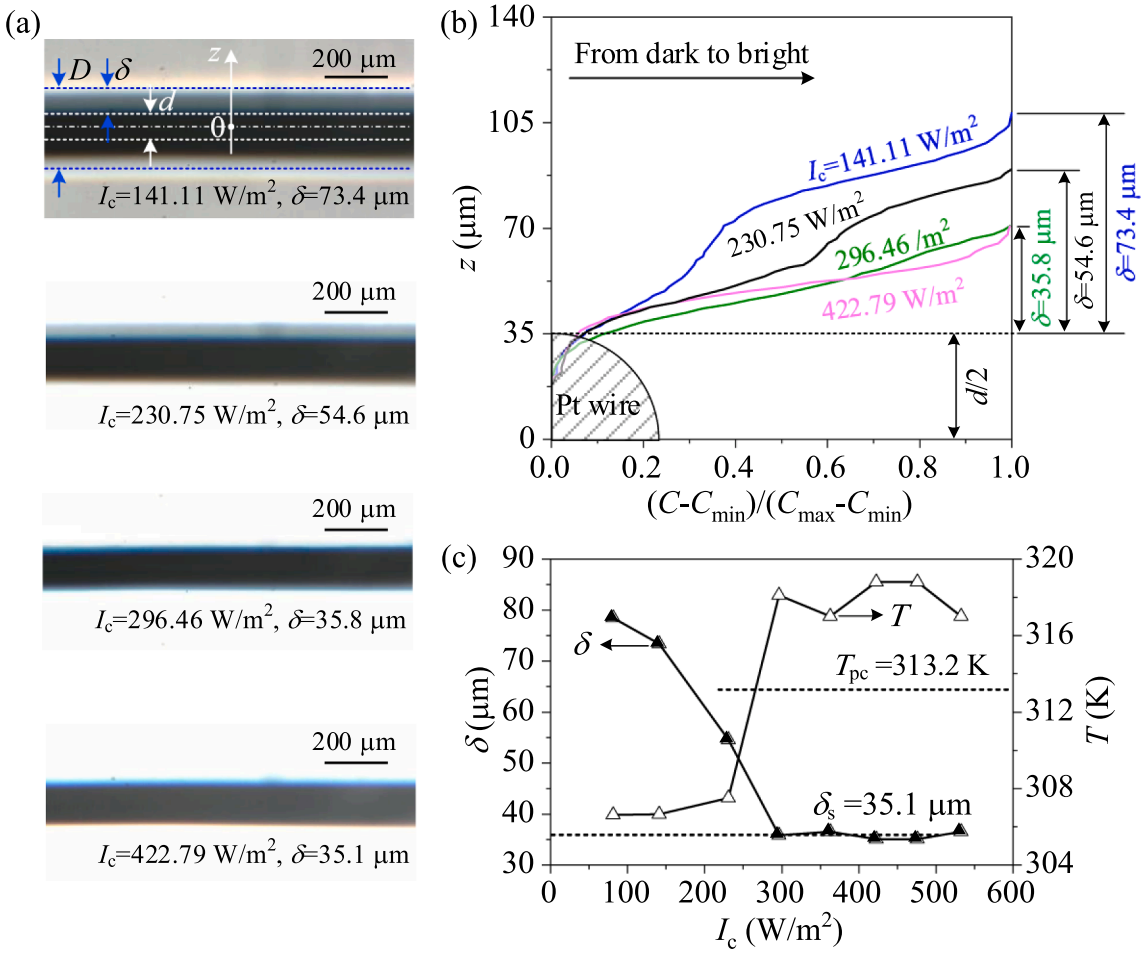


Fig. 4. Pseudo-vapor-layer thickness δ at different irradiance I_c with $P = 9$ MPa, T_b= 306.2 K, T_w= 435.7 K and $q = 302.2$ kW/m^2. (a) Images showing decreased δ with increase of I_c; (b) Determination of δ at different I_c; (c) δ and temperature at the vapor-liquid interface T versus I_c.

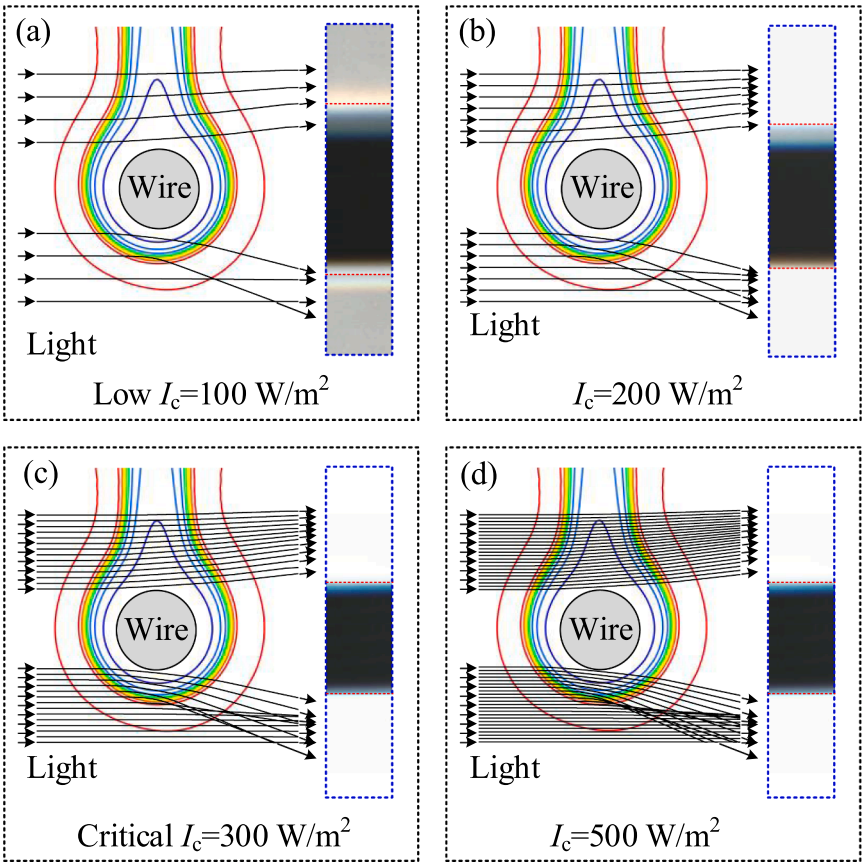


Fig. 5. Explanation of varied δ at different light intensity I_c. (a) I_c= 100 W/m^2; (b) I_c= 200 W/m^2; (c) I_c= 300 W/m^2; (d) I_c= 500 W/m^2.

of 0.075%. An LED light source drives a high-speed camera focused on a 640 × 480 pixel area. The lens enlargement ratio of 300 and 200 corresponds to the spatial resolution of 1.4 μm and 2.4 μm, respectively. The three pressures were controlled to be within (7.582–7.635) MPa, (8.974–9.055) MPa, and (10.976–11.040) MPa, respectively. The heat flux at the wire surface q_L covers a wide range of 0–800 kW/m^2. The errors of q and h can be obtained using the error transmission principle [36], and are 1.58% for q and 3.47% for h. Table 1 summarises the ranges, uncertainties, and response times for various parameters.

3. Results and discussion

3.1. "Boiling" curve in supercritical pressures

The classical theory of natural convection is well established in subcritical pressures [28]. Usually, the Nusselt number *Nu* is correlated with the non-dimensional Rayleigh number *Ra*, giving a monotonous increase of *Nu* with increase of *Ra* [28]. In this work, covering a wide range of wall temperatures of the heater wire, non-monotonic variation of heat transfer coefficients is observed versus wall temperatures, inspiring us to abandon the pure natural convection assumption. Instead, boiling curve widely applied in subcritical pressures is introduced to deal with supercritical heat transfer. In subcritical pressures, heat fluxes and heat transfer coefficients are usually plotted against wall superheating of T_w-T_{sat}, where T_w and T_{sat} are the wall surface temperature and saturation temperature, respectively [37]. An important question arises on *how to define wall superheating in supercritical pressures?* Here, heat transfer is considered in a pseudo-boiling framework. In our previous work [18–20], the analytical model regarding forced convection heat transfer of supercritical fluids in tubes assumes that the interface temperature equals to the pseudo-critical temperature T_{pc}, which is verified by the present measurement. The measured pseudo-interface temperature is ~317 K, which is close to T_{pc}= 313.2 K at P = 9 MPa for a moderate heat flux case of q = 302.2 kW/m^2 and T_w= 435.7 K (see Fig. 4c). It is noted that in supercritical pressures, Hahne et al. [27] presented experimental data on heat fluxes versus wall temperatures. Longmire et al. [38] presented the curve of heat fluxes versus wall temperatures by numerical simulations. The wall superheating was not defined in Refs. [27,38]. He et al. [24] and the present paper clearly define the wall superheating as T_w-T_{pc} in supercritical pressures.

Fig. 6 shows the boiling curves at T_b= 306.2 K with the three pressures of 7.6 MPa, 9.0 MPa and 11.0 MPa, noting that the logarithmic coordinate of q is used in Fig. 6a, and both q and wall superheating ΔT_w cover wide ranges. Indeed, the heat transfer performance is different from that of pure natural convection heat transfer in supercritical

Table 1
Parameters range, uncertainty, and response time.

Parameter	Range	Uncertainty	Response time
pressure P	7.582–11.040 MPa	0.075%	< 100 ms
bulk fluid temperature T_b	288.1–306.3 K	0.2 K	< 250 ms
voltage V	0–6 V	±0.015% + 1 mV	< 1 μs
Platinum wire temperature T_w	288.1–710.5 K	1.13%	< 1 μs
heat flux density q	0–800.5 kW/m^2	1.58%	< 1 μs
heat transfer coefficient h	0–4368.6 kW/(m^2•K)	3.47%	< 1 μs
pseudo-vapor-layer thickness δ_s	0–60.8 μm	1.4 μm(300X) 2.4 μm(200X)	< 250 μs

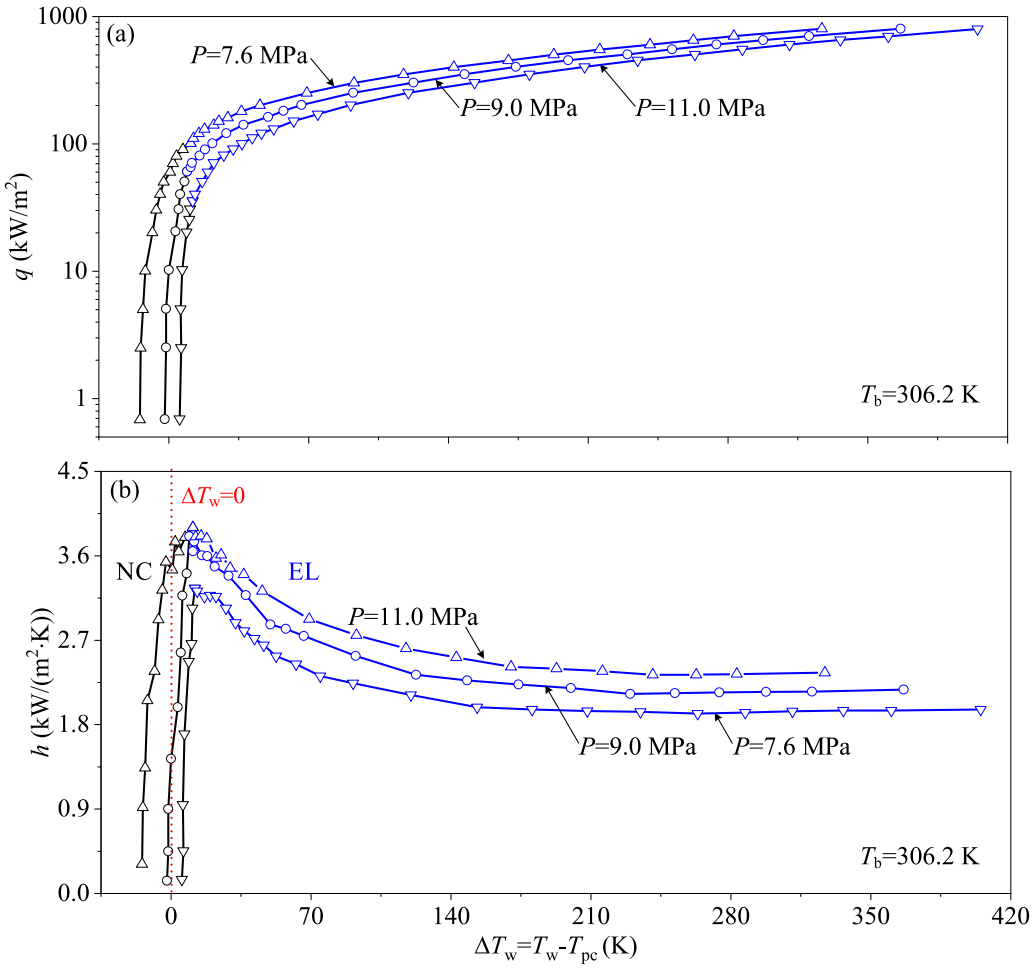


Fig. 6. Heat transfer characteristics of the platinum wire with P = 7.6, 9.0 and 11.0 MPa and T_b= 306.2 K. (a) Pseudo-boiling curve; (b) Heat transfer coefficients h dependent on wall superheating ΔT_w.

pressures. The heat transfer performance can be decoupled into two regions. At small wall superheating such as ΔT_w< 10 K, both q and h

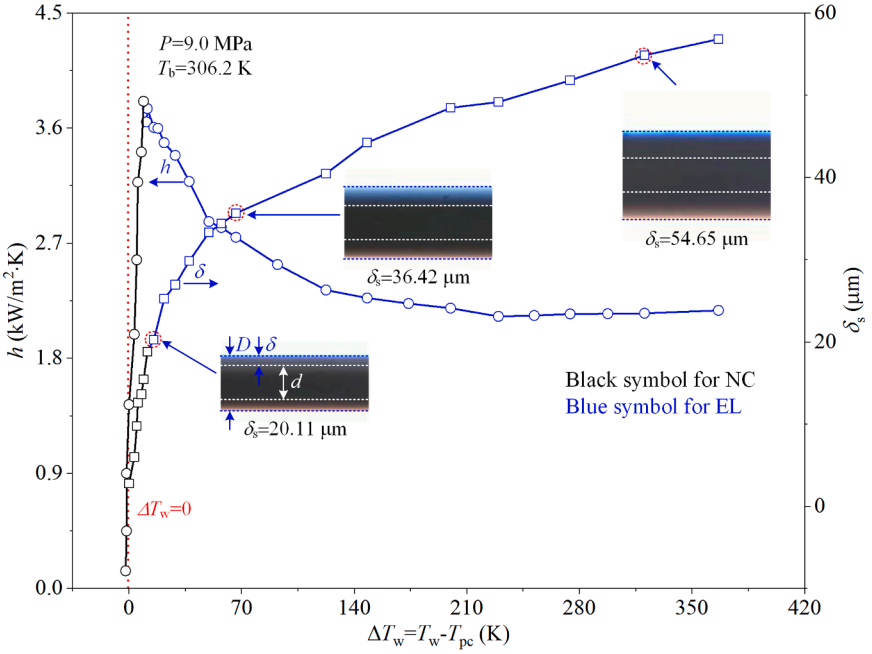


Fig. 7. Heat transfer coefficients h and pseudo-vapor-layer thickness δ_s dependent on wall superheating ΔT_w with P = 9.0 MPa and T_b= 306.2 K.

sharply increase, referred as the first region. The first region is terminated at which the slope of q begins to become gentle and the peak value of h is detected. In the second region with increase of ΔT_w, q continuously rises, but h decreases to approach a constant value. Fig. 6b also indicates the increase trend of heat transfer coefficients with increase of pressures from 7.6 MPa to 11.0 MPa, which will be explained later.

Fig. 7 links heat transfer coefficients and pseudo-vapor-layer thickness. It is interesting to note that in the first region, both heat transfer coefficients and pseudo-vapor-layer thicknesses sharply increase. Due to significant low thermal conductivity in the pseudo-vapor-layer, the pseudo-vapor-layer introduces an additional thermal resistance to deteriorate heat transfer. Because even though the pseudo-vapor-layer thicknesses increase, the heat transfer coefficients still rise, concluding the natural convection dominated mechanism with weak effect of the pseudo-vapor-layer heat transfer.

Because significant pseudo-vapor-layer is observed beyond the peak heat transfer coefficient, the second region is termed the evaporation-like region. The physical picture in this region behaves as the combined pseudo-vapor-layer heat transfer mechanism and natural convection heat transfer mechanism, where the latter takes place beyond the pseudo-interface. On the one hand, with increase of wall superheating, the increased pseudo-vapor-layer thickness deteriorates heat transfer. On the other hand, the increased wall superheating enhances natural convection heat transfer. The heat transfer performance in the second region reflects the comprehensive balance between pseudo-vapor-layer effect and the natural convection effect.

Figs. 6–7 identify distinct difference regarding boiling heat transfer in two different pressure domains. In supercritical pressures, constant heat transfer coefficient at ultra-high wall superheating is caused by the comprehensive effect of vapor-like heat transfer and natural convection heat transfer. At high wall superheating or heat fluxes, stable heat transfer can be maintained, under which the heater may not be burned out if the tolerance temperature of the material is higher than the stable wall temperature at the corresponding heat flux. Otherwise, it will be destroyed if the tolerance temperature of the material is lower than the stable temperature at the corresponding heat flux. In subcritical pressures, on the contrary, boiling heat transfer displays film boiling characteristic at high heat fluxes [37]. A pseudo-vapor-layer exists on the heater surface. Large bubbles ejection from the pseudo-vapor-layer induces interfacial Rayleigh-Taylor instability [37]. If the dissipated vapor of these bubbles is smaller than the generated vapor on the heater surface, the pseudo-vapor-layer quickly increases versus time to cause un-controllable temperature rise of the heater materials, resulting in burnout of the heater [39]. It is seen that burnout in subcritical pressures is a time-dependent phenomenon, where a negative feedback mechanism cannot be established under ultra-high heat flux conditions, contrary to the well-established negative feedback mechanism under supercritical pressure. In supercritical pressures, the negative feedback mechanism refers to enhanced natural convection heat transfer compensated by deteriorated heat transfer due to increased pseudo-vapor-layer thickness, accounting for constant heat transfer coefficient at high heating intensities.

It is noted that Fig. 4 and Figs. 6–7 refer to two different phenomena. Fig. 4 shows that for a given case with $P = 9$ MPa, $T_b = 306.2$ K, $T_w = 435.7$ K and $q = 302.2$ kW/m^2, the pseudo-vapor-layer thickness δ varies with the light intensity of the lamp I_c. As I_c continuously increases, δ decreases until it reaches a constant value δ_s, which is used for heat transfer analysis. Figs. 6–7 illustrate the heat transfer coefficients h and the saturated pseudo-vapor-layer thickness δ_s as functions of wall superheating under different operating conditions. Beyond the maximum point, h decreases to approach a constant value, which is caused by the increased natural convection enhancing heat transfer and the increased pseudo-vapor-layer thickness deteriorating heat transfer as wall superheating increases.

3.2. Effect of pressures on supercritical heat transfer

Experimental studies on supercritical heat transfer focus on the near-critical pressure region [26,27,40–42]. Experiment data with pressures significantly higher than the critical value are scarce. Recently, to develop advanced sCO_2 power generation technology, convection heat transfer has been experimentally investigated in a wide range of P_c~$3P_c$ [18–20], where P_c is the critical pressure. Both NHT and HTD are identified [18–20]. Usually, the HTD takes place at high heat flux and/or low mass flux, under which wall temperatures of the tube have a steep increase followed by a recovery trend. In the single-phase fluid framework, supercritical heat transfer is dealt with by considering the buoyancy effect and acceleration effect [2,3]. However, the single-phase fluid assumption fails to predict both the normal heat transfer and HTD [4,5]. To better understand forced convection heat transfer in supercritical pressures, a physical picture is proposed to include a pseudo-vapor-layer on the wall surface and a core fluid region. The two regions are interfaced at the pseudo-critical temperature. The force analysis applied on the pseudo-interface yields the *SBO* and *K* number, reflecting the competition between the evaporation induced momentum force and inertia force, governing the growth of pseudo-vapor-layer which is success to deal with forced convection heat transfer of supercritical fluids [18–20].

The *SBO* is expressed as $SBO = q/(Gi_{pc})$, where q is the heat flux, G is the mass flux and i_{pc} is the enthalpy at the pseudo-critical temperature [18]. The number successfully explains the improved performance of forced convection heat transfer of supercritical fluids [18]. When this number is introduced to treat the immersion heat transfer of supercritical fluids, a challenge exists to determine the mass flux. By neglecting the mass flux effect, we temporarily use the term q/i_{pc} to quantify the relative contribution of heat flux effect and the pressure effect on the heat transfer. Fig. 8 plots the effect of pressures on heat transfer coefficients h, saturation pseudo-vapor-layer thickness δ_s, and the parameter of q/i_{pc}, indicating that the elevated heat transfer at higher pressures is indeed caused by the decreased pseudo-vapor-layer thickness and the parameter of q/i_{pc}. This pressure effect is induced by the raised enthalpy i_{pc} when pressure increases.

3.3. Contribution of pseudo-vapor-layer heat transfer

Here, we quantify the contribution of the pseudo-vapor-layer to the immersion heat transfer of supercritical fluids, using the physical picture shown in Fig. 9a. Beyond the cylinder heater wire, there are a pseudo-vapor-layer with the thickness of δ_s and a bulk fluid region whose temperatures are in the range of T_{pc} and T_b. The wire surface temperature is T_w while the interface temperature is T_{pc}. Based on this picture, the total thermal resistance R_t consists of two parts of R_{VL} and R_{NC},

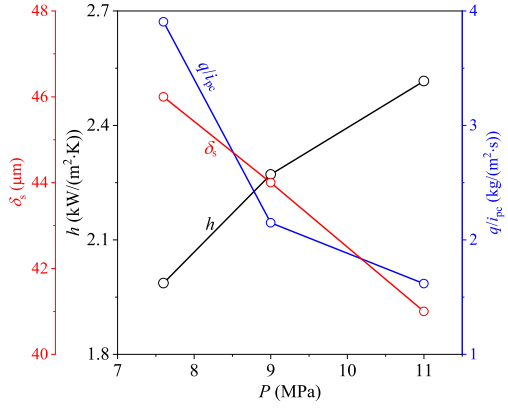


Fig. 8. Effect of pressure on heat transfer coefficient h, pseudo-vapor-layer thickness δ_s and q/i_{pc} at $T_b = 306.2$ K and $q = 302.21$ kW/m^2.

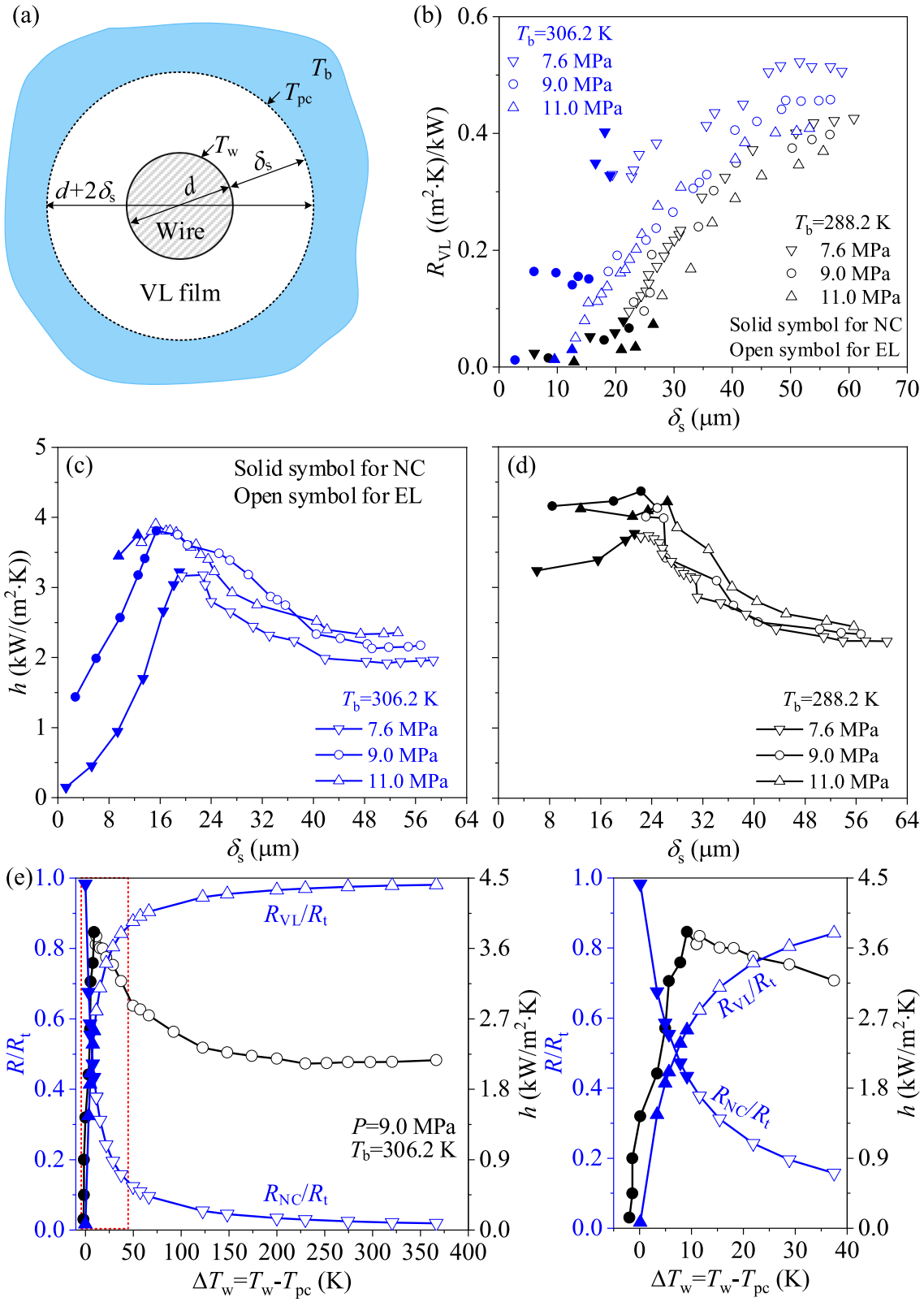


Fig. 9. Contribution of pseudo-vapor-layer heat transfer. (a) Physical picture of heat transfer; (b) Pseudo-vapor-layer resistances R_{VL} depend on pseudo-vapor-layer thickness δ_s; (c) and (d) Overall heat transfer coefficients h depend on δ_s; (e) The pseudo-vapor-layer resistance R_{VL} and natural convection resistance R_{NC} contributed to the total thermal resistance R_t with P = 9.0 MPa and T_b= 306.2 K.

which are written as

$$R_t = R_{VL} + R_{NC}, \quad R_t = \frac{T_w - T_b}{q}, \quad R_{VL} = \frac{T_w - T_{pc}}{q} \tag{9}$$

Where the subscripts of VL and NC represent pseudo-vapor-layer and natural convection, respectively. By Eq. (9), a new parameter, termed the pseudo-vapor-layer contribution ratio β is defined as

$$\beta = \frac{R_{VL}}{R_t} = \frac{T_w - T_{pc}}{T_w - T_b} \tag{10}$$

On the other hand, the conduction thermal resistance of pseudo-vapor-layer is computed as [43]

$$R_{VL,con} = \frac{d\ln[(d + 2\delta_s)/d]}{2\lambda_{ave}} \tag{11}$$

Where d is the heater diameter, λ_{ave} is the average thermal conductivity of pseudo-vapor-layer with temperatures from T_w to T_{pc}, which is as follows [44]

$$\lambda_{ave} = \frac{1}{T_w - T_{pc}} \int_{T_{pc}}^{T_w} \lambda(T) dT \tag{12}$$

Fig. 9b plots the pseudo-vapor-layer resistances influenced by the saturation pseudo-vapor-layer thickness, noting that the solid and open symbols represent the data in the first region (natural convection region) and the second region (evaporation-like region), respectively, showing the increased pseudo-vapor-layer resistances with increases of pseudo-vapor-layer thicknesses. At the same δ_s, the higher bulk fluid temperature of T_b= 306.2 K elevates the pseudo-vapor-layer resistance. The link between the overall heat transfer coefficients and pseudo-vapor-layer thicknesses is shown in Fig. 9c with T_b= 306.2 K and Fig. 9d with T_b= 288.2 K, respectively. It is seen that both h and δ_s raise in the first region. However, h decreases to approach constant with continuous increase of δ_s in the second region.

Fig. 9e quantifies the pseudo-vapor-layer resistance and natural convection resistance contributed to the total thermal resistance. Two extreme conditions are considered here. At very small wall superheating such as ΔT_w< 5 K, natural convection mechanism dominates heat transfer, but R_{NC}/R_t quickly decreases with increase of ΔT_w. At ultra-high wall superheating such as ΔT_w> 200 K, the pseudo-vapor-layer contributes > 95% of the total thermal resistance, with weak contribution of natural convection beyond the T_{pc} interface. On the moderate wall superheating such as 10 K< ΔT_w< 100 K, both natural convection mechanism and pseudo-vapor-layer heat transfer mechanism are important to be competed with each other.

Previously, the immersion heat transfer of supercritical fluids is treated using the similar way of pure natural convection in subcritical pressures [40–42]. Our work emphasizes the importance of the pseudo-vapor-layer on the immersion heat transfer of supercritical CO_2. The pseudo-vapor-layer contribution ratio β defined in Eq. (10) is suggested to be a new non-dimensional parameter to quantify the significance of the pseudo-vapor-layer heat transfer. Now, our attention is paid on the inside of the pseudo-vapor-layer envelope. Previous work assumes the pure conduction heat transfer in the layer [45]. Because the conduction resistance of pseudo-vapor-layer can be predicted by Eqs. (11) and (12), the ratio of conduction resistance relative to overall resistance of pseudo-vapor-layer, $R_{VL,con}/R_{VL}$, is plotted in Fig. 10, which can be 10 at very small wall superheating, but attains ~2.4 at high wall superheating such as ΔT_w> 200 K. Fig. 10 indicates that the conduction heat transfer assumption over-estimates the thermal resistance of pseudo-vapor-layer, due to the vapor flow effect in the pseudo-vapor-layer (see the insert figure in Fig. 10).

4. Conclusion

Conclusions of the present paper is summarized as follows:

(1) Immersion heat transfer of sCO_2 was experimentally studied, with pressures significantly higher than the critical pressure. Covering a wide range of heat fluxes up to 800 kW/m^2, heat transfer coefficients sharply increase to a peak value, then decrease to reach a constant value.
(2) The pseudo-vapor-layer interface is captured using a high-speed camera and grey extraction approach. For a specific run, the pseudo-vapor-layer thicknesses decrease with increase of irradiance power, but a saturation value can be reached, eliminating uncertainties when using different light power sources.
(3) At very small wall superheating, both heat transfer coefficients and pseudo-vapor-layer thicknesses are increased. The enlarged pseudo-vapor-layer does not deteriorate heat transfer, indicating weak effect of pseudo-vapor-layer heat transfer in this region.

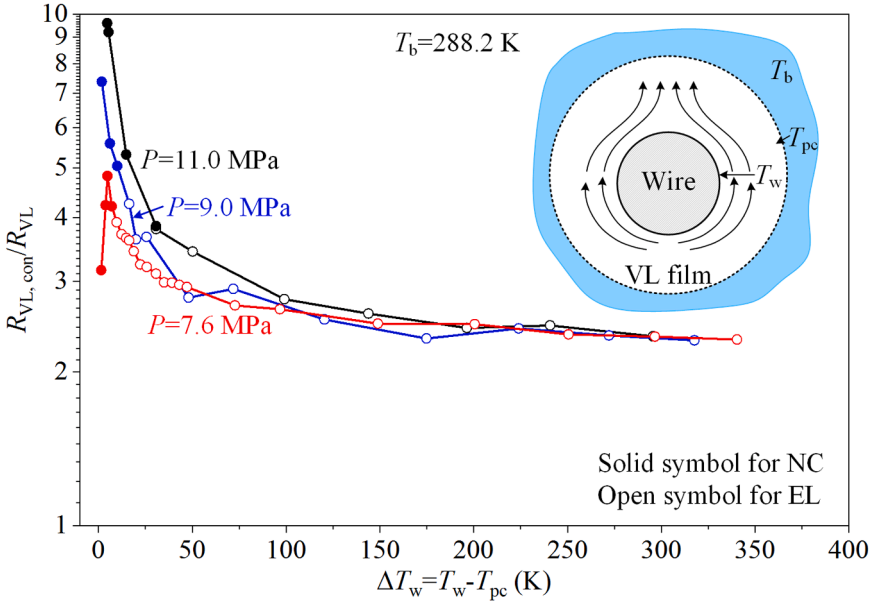


Fig. 10. Ratio $R_{VL,\ con}/R_{VL}$ (conduction to overall pseudo-vapor-layer resistance) vs. wall superheating ΔT_w with P = 7.6, 9.0 and 11.0 MPa and T_b= 288.2 K.

(4) Beyond the peak point of heat transfer coefficient, heat transfer coefficients decrease to approach a constant value. Meanwhile, the pseudo-vapor-layer thicknesses increase, indicating the increased significance of pseudo-vapor-layer heat transfer.
(5) In the moderate wall superheating, both natural convection and pseudo-vapor-layer heat transfer are competed to yield a comprehensive heat transfer coefficient. A non-dimensional parameter is proposed to characterize the pseudo-vapor-layer contribution on the supercritical heat transfer.
(6) The pseudo-vapor-layer contains both mechanisms of conduction and convection. The conduction assumption in the pseudo-vapor-layer overestimates the thermal resistance of pseudo-vapor-layer.

CRediT authorship contribution statement

Xiongjiang Yu: Writing – review & editing, Resources. **Jinliang Xu:** Writing – review & editing, Writing – original draft, Supervision, Resources, Methodology, Funding acquisition. **Guanglin Liu:** Methodology, Investigation. **Jian Xie:** Supervision, Investigation. **Bo Zhang:** Writing – original draft, Visualization, Investigation, Formal analysis, Data curation.

Declaration of Competing Interest

The authors declare that they have no known competing financial interests or personal relationships that could have appeared to influence the work reported in this paper.

Acknowledgments

The authors acknowledge the support from the National Natural Science Foundation of China (No. 52130608 and No. 52206197).

Data availability

Data will be made available on request.

References

[1] Y. Cengel, M. Boles. Thermodynamics: An Engineering Approach, 6th ed., McGraw-Hill, New York, 2006.
[2] J.D. Jackson, M.A. Cotton, B.P. Axcell, Studies of mixed convection in vertical tubes, Int. J. Heat. Fluid. Flow. 10 (1989) 2–15, https://doi.org/10.1016/0142-727X(89)90049-0.
[3] D. McEligot, C. Coon, H. Perkins, Relaminarization in tubes, Int. J. Heat. Mass. Transf. 13 (1970) 431–433, https://doi.org/10.1016/0017-9310(70)90118-3.
[4] Q. Wang, J. Xu, C. Zhang, B. Hao, L. Cheng, A critical review on heat transfer of supercritical fluids, Heat. Transf. Eng. 44 (2023) 1969–1994, https://doi.org/10.1080/01457632.2022.2164684.
[5] R. Xiao, L. Chen, Y. Hou, C. Du, Y. Cai, Experimental study on heat transfer behavior and prediction of heat transfer deterioration of supercritical nitrogen in vertical tubes, Int. Commun. Heat. Mass. Transf. 155 (2024) 107467,, https://doi.org/10.1016/j.icheatmasstransfer.2024.107467.
[6] A. Alasif, A. Pucciarelli, O. Siddiqui, A. Shams, An overview of the prediction methods for the heat transfer of supercritical fluids, Prog. Nucl. Energy 181 (2025) 105654, https://doi.org/10.1016/j.pnucene.2025.105654.
[7] M. Pizzarelli, The status of the research on the heat transfer deterioration in supercritical fluids: a review, Int. Commun. Heat. Mass. Transf. 95 (2018) 132–138, https://doi.org/10.1016/j.icheatmasstransfer.2018.04.006.
[8] I.L. Pioro, R.B. Duffey, Experimental heat transfer in supercritical water flowing inside channels (survey), Nucl. Eng. Technol. 235 (2005) 2407–2430, https://doi.org/10.1016/j.nucengdes.2005.05.034.
[9] J.P. Holman, S.N. Rea, C.E. Howard, Forced convection heat transfer to Freon 12 near the critical state in a vertical annulus, Int. J. Heat. Mass. Transf. 8 (1965) 1095–1102, https://doi.org/10.1016/0017-9310(65)90137-7.
[10] J.W. Ackerman, Pseudoboiling heat transfer to supercritical pressure water in smooth and ribbed tubes, J. Heat. Transf. 92 (1970) 490–497, https://doi.org/10.1115/1.3449698.
[11] P. Gallo, D. Corradini, M. Rovere, Widom line and dynamical crossovers as routes to understand supercritical water, Nat. Commun. 5 (2014) 5806, https://doi.org/10.1038/ncomms6806.
[12] F. Maxim, C. Contescu, P. Boillat, B. Niceno, K. Karalis, A. Testino, C. Ludwig, Visualization of supercritical water pseudo-boiling at Widom line crossover, Nat. Commun. 10 (2019) 4114, https://doi.org/10.1038/s41467-019-12117-5.
[13] D.T. Banuti, Crossing the Widom-line–supercritical pseudo-boiling, J. Supercrit. Fluids 98 (2015) 12–16, https://doi.org/10.1016/j.supflu.2014.12.019.
[14] F. Simeski, M. Ihme, Supercritical fluids behave as complex networks, Nat. Commun. 14 (2023) 1996, https://doi.org/10.1038/s41467-023-37645-z.
[15] J. Xu, Y. Wang, X. Ma, Phase distribution including a bubblelike region in supercritical fluid, Phys. Rev. E 104 (2021) 014142, https://doi.org/10.1103/PhysRevE.104.014142.
[16] M.Y. Ha, T.J. Yoon, T. Tlusty, Y. Jho, W.B. Lee, Widom delta of supercritical gas-liquid coexistence, J. Phys. Chem. Lett. 9 (7) (2018) 1734–1738, https://doi.org/10.1021/acs.jpclett.8b00430.
[17] Q. Wang, X. Ma, J. Xu, M. Li, Y. Wang, The three-regime-model for pseudo-boiling in supercritical pressure, Int. J. Heat. Mass. Transf. 181 (2021) 121875, https://doi.org/10.1016/j.ijheatmasstransfer.2021.121875.
[18] B. Zhu, J. Xu, X. Wu, J. Xie, M. Li, Supercritical "boiling" number, a new parameter to distinguish two regimes of carbon dioxide heat transfer in tubes, Int. J. Therm. Sci. 136 (2019) 254–266, https://doi.org/10.1016/j.ijthermalsci.2018.10.032.
[19] J. Xu, H. Zhang, B. Zhu, J. Xie, Critical supercritical-boiling-number to determine the onset of heat transfer deterioration for supercritical fluids, Sol. Energy 195 (2020) 27–36, https://doi.org/10.1016/j.solener.2019.11.036.
[20] B. Zhu, J. Xu, C. Yan, J. Xie, The general supercritical heat transfer correlation for vertical up-flow tubes: *K* number correlation, Int. J. Heat. Mass. Transf. 148 (2020) 119080, https://doi.org/10.1016/j.ijheatmasstransfer.2019.119080.
[21] J.V. Nieuwenhuyse, S. Lecompte, M.D. Paepe, Development of a general heat transfer correlation for horizontal flow of supercritical low GWP refrigerants under heating conditions, Int. J. Heat. Mass. Transf. 252 (2025) 127398, https://doi.org/10.1016/j.ijheatmasstransfer.2025.127398.
[22] H. Pu, H. Chang, J. Wang, Y. Shang, M. Dong, S. Li, Experimental investigation and analysis of convective heat transfer to supercritical pressure aviation kerosene RP-3 in vertical miniature tubes based on the pseudo-boiling theory, Appl. Therm. Eng. 219 (2023) 119651, https://doi.org/10.1016/j.applthermaleng.2022.119651.
[23] S. Kandlikar, M. Shoji, V. Dhir. Handbook of Phase Change: Boiling and Condensation, Talyor & Francis, Philadelphia, 1999.
[24] X. He, J. Xu, X. Yu, J. Xie, Distinguishing evaporation-like and boiling-like modes of pseudo-boiling in supercritical pressures, Int. J. Heat. Mass. Transf. 214 (2023) 124417, https://doi.org/10.1016/j.ijheatmasstransfer.2023.124417.
[25] X. He, J. Xu, J. Xie, Quantitative characterization of the pseudo-boiling contribution to supercritical heat transfer, Phys. Fluids 36 (2024) 013343, https://doi.org/10.1063/5.0187146.
[26] K.K. Knapp, R.H. Sabersky, Free convection heat transfer to carbon dioxide near the critical point, Int. J. Heat. Mass. Transf. 9 (1966) 41–51, https://doi.org/10.1016/0017-9310(66)90055-X.
[27] E. Hahne, R. Neumann, Boiling-like phenomena in free-convection heat transfer at supercritical pressures, Wärme-und Stoffübertrag. 15 (1981) 171–180, https://doi.org/10.1007/BF01376829.
[28] W.M. Rohsenow, J.P. Hartnett, Y.I. Cho. Handbook of Heat Transfer, 3th ed., Mcgraw-hill, New York, 1998.
[29] B. Zappoli, D. Beysens, Y. Garrabos. Heat Transfers and Related Effects in Supercritical Fluids, Springer, New York, 2015.
[30] J. Xu, E. Sun, M. Li, H. Liu, B. Zhu, Key issues and solution strategies for supercritical carbon dioxide coal fired power plant, Energy 157 (2018) 227–246, https://doi.org/10.1016/j.energy.2018.05.162.
[31] N. Mazaheri, A. Mwesigye, Novel high heat flux thermal management with combined supercritical CO_2 and a microjet heat sink, Appl. Therm. Eng. 256 (2024) 124143, https://doi.org/10.1016/j.applthermaleng.2024.124143.
[32] E. Reverchon, R. Adami, Nanomaterials and supercritical fluids, J. Supercrit. Fluids 37 (2006) 1–22, https://doi.org/10.1016/j.supflu.2005.08.003.
[33] H. Erkonak, O.Ö. Söğüt, M. Akgün, Treatment of olive mill wastewater by supercritical water oxidation, J. Supercrit. Fluids 46 (2008) 142–148, https://doi.org/10.1016/j.supflu.2008.04.006.
[34] M. Selmke, Bubble optics, Appl. Opt. 59 (2019) 45–58, https://doi.org/10.1364/AO.59.000045.
[35] M.V. Avdeev, A.N. Konovalov, V.N. Bagratashvili, V.K. Popov, S.I. Tsypina, M. Sokolova, J. Ke, M. Poliakoff, The fibre optic reflectometer: a new and simple probe for refractive index and phase separation measurements in gases, liquids and supercritical fluids, PCCP 6 (2004) 1258–1263, https://doi.org/10.1039/B311207A.
[36] R.J. Moffat, Describing the uncertainties in experimental results, Exp. Therm. Fluid. Sci. 1 (1988) 3–17, https://doi.org/10.1016/0894-1777(88)90043-X.
[37] V.P. Carey. Liquid-Vapor Phase-Change Phenomena: An Introduction to the Thermophysics of Vaporization and Condensation Processes in Heat Transfer Equipment, 3rd ed., CRC Press, Boca Raton, 2020.
[38] N.P. Longmire, D.T. Banuti, Onset of heat transfer deterioration caused by pseudo-boiling in CO_2 laminar boundary layers, Int. J. Heat. Mass. Transf. 193 (2022) 122957, https://doi.org/10.1016/j.ijheatmasstransfer.2022.122957.
[39] G. Liang, I. Mudawar, Pool boiling critical heat flux (CHF)-Part 1: review of mechanisms, models, and correlations, Int. J. Heat. Mass. Transf. 117 (2018) 1352–1367, https://doi.org/10.1016/j.ijheatmasstransfer.2017.09.134.
[40] R.J. Neumann, E.W. Hahne, Free convective heat transfer to supercritical carbon dioxide, Int. J. Heat. Mass. Transf. 23 (1980) 1643–1652, https://doi.org/10.1016/0017-9310(80)90223-9.
[41] Y. Rousselet, G.R. Warrier, V.K. Dhir, Natural convection from horizontal cylinders at near-critical pressures—part I: experimental study, J. Heat. Transf. 135 (2013) 022501, https://doi.org/10.1115/1.4007672.
[42] G.R. Warrier, Y. Rousselet, V.K. Dhir, Natural convection from horizontal cylinders at near-critical pressures—part II: numerical simulations, J. Heat. Transf. 135 (2013) 022502, https://doi.org/10.1115/1.4007673.

[43] T.L. Bergman, A.S. Lavine. Fundamentals of Heat and Mass Transfer, 8th ed., John Wiley & Sons, Inc., Hoboken, 2017.
[44] H. Kato, N. Nishiwaki, M. Hirata, Studies on the heat transfer of fluids at a supercritical pressure: 1st report, a proposition of reference values of thermal properties and experiments with supercritical carbon-dioxide, Bull. JSME 11 (1968) 654–663, https://doi.org/10.1299/jsme1958.11.654.
[45] C. Yan, Y. Zhang, X. Zhang, W. Wang, B. Zhao, Numerical study on natural convection heat transfer of supercritical CO_2 in an infinite space, Int. J. Heat. Mass. Transf. 156 (2024) 107680, https://doi.org/10.1016/j.icheatmasstransfer.2024.107680.